PNAS RESEARCH ARTICLE | CHEMISTRY

Unveiling the mechanism for selective cleavage of C-C bonds in sugar reactions on tungsten trioxide–based catalysts

Yue Liu[a,1], Wei Zhang[a,1], Cong Hao[b], Shuai Wang[b], and Haichao Liu[a,2]

Edited by Alexis Bell, University of California, Berkeley, CA; received April 12, 2022; accepted July 5, 2022

Conversion of naturally occurring sugars, the most abundant biomass resources on Earth, to fuels and chemicals provides a sustainable and carbon-neutral alternative to the current fossil resource–based processes. Tungsten-based catalysts (e.g., WO_3) are efficient for selectively cleaving C-C bonds of sugars to $C_{2,3}$ oxygenate intermediates (e.g., glycolaldehyde) that can serve as platform molecules with high viability and versatility in the synthesis of various chemicals. Such C-C bond cleavage follows a mechanism distinct from the classical retro-aldol condensation. Kinetic, isotope ^{13}C-labeling, and spectroscopic studies and theoretical calculations, reveal that the reaction proceeds via a surface tridentate complex as the critical intermediate on WO_3, formed by chelating both α- and β-hydroxyls of sugars, together with the carbonyl group, with two adjacent tungsten atoms (W-O-W) contributing to the β-C-C bond cleavage. This mechanism provides insights into sugar chemistry and enables the rational design of catalytic sites and reaction pathways toward the efficient utilization of sugar-based feedstocks.

reaction mechanism | C-C bond cleavage | sugar | glucose | WO_3

Sugars (i.e., carbohydrates) are the naturally occurring products from CO_2 and H_2O via photosynthesis, and they constitute the most abundant renewable carbon resources on Earth. They are readily available from forest and agricultural waste. As such, sugars have become the most promising alternatives to the diminishing fossil resources for the sustainable production of fuels and chemicals toward the global goal of carbon neutrality. To this end, various chemical and biochemical conversion routes of sugars have been developed (1–7), such as hydrogenation and hydrogenolysis to sorbitol, ethylene glycol, and propylene glycol (3); amination to aminopolyols (4); dehydration to furfurals and derivatives (5); and conversion to carboxylic acids (6, 7). However, most of these routes, particularly to chemicals, rely on specific sugars as the reactants, which are generally obtained from natural biomass sources via tedious and energy-intensive separation and purification because of the structural complexity of sugars, in terms of their chiralities, carbon numbers, types (i.e., ketoses and aldoses), and conformational diversities of cyclic structures (i.e., α-/β-furanoses and α-/β-pyranoses). This problem presents significant hurdles to the practical applications of sugars as versatile feedstocks.

Inspired by the petrochemical industry, in which $C_{2,3}$ olefins (i.e., ethylene and propylene) serve as the building blocks for the production of various chemicals, irrespective of the sources and compositions of the crude oils (*SI Appendix*, Scheme S1), $C_{2,3}$ oxygenate intermediates (e.g., glycolaldehyde and glyceraldehyde) can be considered to play similar roles in the conversion of sugars to chemicals (8). In this scenario, the primary step is to develop a reaction process capable of converting the different sugar molecules to the $C_{2,3}$ oxygenate intermediates regardless of their structural diversities, in analogy to the steam cracking or catalytic cracking of C_{2+} hydrocarbons (e.g., liquid petroleum gas and naphtha) to ethylene and propylene in the petrochemical industry (*SI Appendix*, Scheme S1). Since most natural sugars consist of five and six carbon atoms, as represented by glucose and xylose, controllable breaking of their C-C bonds is critical for cracking them to the $C_{2,3}$ oxygenate intermediates.

Such C-C bond cleavage is conventionally catalyzed by bases (e.g., NaOH) via retro-aldol condensation, but it is not easy to control the selectivity and integrate with other reactions due to the high reactivity of the sugar reactants and intermediates with bases (9, 10). In recent years, a series of tungsten-based catalysts, such as W_2C, H_2WO_4, and WO_3, have shown superior efficiencies for the conversion of sugars to the $C_{2,3}$ intermediates ($C_2H_4O_2$ and $C_3H_6O_3$) (11–15), which, in coupling with different reactions, subsequently react to form a variety of products, such as ethylene glycol (11, 12, 15–17), propylene glycol (13, 18, 19), ethanol (20–23), and lactic acid (24). Extensive studies on this sugar reaction have led to significant progress in the understanding of kinetics (25–28) and active sites (13, 19, 29, 30), optimization of catalytic

Significance

Sugars are carbon-neutral alternatives to fossil resources for the sustainable production of fuels and chemicals. Their direct conversion is challenged by their structural complexities of different chiralities, carbon numbers, and types of ketoses/aldoses and by their tedious purification. WO_3-catalyzed cracking of sugars provides a viable strategy to convert them, irrespective of their purities and structures, primarily to $C_{2,3}$ oxygenate intermediates (e.g., glycolaldehyde) that can be used as building blocks, resembling the strategy in the current petrochemical industry, to synthesize various chemicals. This work unveils the mechanism for selective cleavage of β-C-C bonds of sugar on WO_3, providing insights into sugar chemistry and a rationale for the design of catalysts and reaction pathways for the production of chemicals from sugar-based biomass.

Author contributions: H.L. designed research; Y.L., W.Z., C.H. and S.W. performed research; Y.L., W.Z., and H.L. analyzed data; and Y.L., W.Z., C.H., S.W., and H.L. wrote the paper.

The authors declare no competing interest.

This article is a PNAS Direct Submission.

[1]Y.L. and W.Z. contributed equally to this work.

[2]To whom correspondence may be addressed. Email: hcliu@pku.edu.cn.

This article contains supporting information online at http://www.pnas.org/lookup/suppl/doi:10.1073/pnas.2206399119/-/DCSupplemental.

Published August 19, 2022.

performances and recyclability (17, 26, 31–34), and applicability to different substrates (35–37). However, it is still not clear how the C-C bonds of sugars are selectively cleaved on the tungsten-based catalysts, such a central step in the conversion of sugars to chemicals with high efficiency and versatility.

Several reports have proposed C-C bond cleavage via acidic WO_3-catalyzed retro-aldol condensation, based on results showing that the reaction occurs selectively at the β-position to the carbonyl group of sugars (15, 22, 23, 30, 38). However, this retro-aldol mechanism cannot explain the indispensable requirements, as we preliminarily reported, for the α-hydroxyl group of sugars and the aggregated tungsten species as the catalytic sites (e.g., crystalline rather than highly dispersed WO_3) (13). Moreover, other typical acid catalysts—mineral acids (39), H-form zeolites (40, 41), and sulfonated carbons (41, 42)—are inactive for this C-C bond β-scission reaction. Therefore, selective cleavage of C-C bonds in sugars reflects a unique property of the tungsten-based catalysts, on which the reaction does not follow the classical retro-aldol condensation mechanism.

In this work, we use WO_3 as a model catalyst and explore the reaction mechanism for selective cleavage of C-C bonds of various $C_{4–6}$ sugars, including aldoses, ketoses, and deoxysugars for comparison. By examining the structural effects of sugars on the activities, product distributions, and reaction intermediates using a combination of kinetic, isotope ^{13}C-labeling, and spectroscopic methods and theoretical calculations, we find that the reaction on the WO_3 surface proceeds via a sugar-WO_3 tridentate complex, involving the coordination of both α- and β-hydroxyl groups, together with the carbonyl group, with adjacent tungsten sites. This mechanism enables us to elucidate the structural requirements of sugars and tungsten-based catalysts for the selective C-C bond cleavage and consequently to tune the corresponding catalytic sites and reaction pathways.

Results and Discussion

Selective Cleavage of C-C Bonds for Different Sugars on WO_3. Conversion of glucose to ethylene glycol was first examined as a model reaction to probe the C-C bond cleavage of sugars. This reaction requires catalytic functions for the C-C cleavage and the consequent intermediate hydrogenation. As shown in Table 1, with only hydrogenation catalyst of Ru/C, glucose (present in its D-configuration, i.e., D-glucose, if not specifically mentioned) was hydrogenated to sorbitol (70.3%) with a trivial amount of ethylene glycol (9.3%) at 205 °C and 6 MPa of H_2 in 10 min (Table 1, entry 1). The formation of ethylene glycol was due to the thermal decomposition of glucose at such a high temperature, followed by hydrogenation (43). Other products included mannitol (7.4%), pentitols (3.5%), propylene glycol (6.1%), and glycerol (1.9%). Upon addition of WO_3, ethylene glycol became the major product, and its yield increased from 9.3 to 59.4%, while sorbitol yield concurrently decreased from 70.3 to 9.2% (Table 1, entry 2). It is known that ethylene glycol can be formed from hydrogenolysis of polyols in the presence of bases (44, 45). However, this reaction did not occur under the conditions in this work when sorbitol and xylitol were directly used as the reactants (*SI Appendix*, Table S1). For comparison, other metal oxides with different surface acidity and basicity (Nb_2O_5, TiO_2, ZrO_2, and Al_2O_3) and also different reducibility (V_2O_5, MnO_2, and MoO_3) were examined. Use of Nb_2O_5 hardly showed obvious changes in the product distributions compared to those in its absence (Table 1, entry 3). On TiO_2, ZrO_2, and Al_2O_3, the ethylene glycol yield increased to 19.9 to 23.6% as a result of their surface basic site-catalyzed retro-aldol condensation of glucose, but sorbitol was still the dominant product, with yields of 54.5 to 61.6% (Table 1, entries 4–6). On reducible V_2O_5, MnO_2, and MoO_3, very few polyols but a large amount of humin by-products were detected (Table 1, entries 7–9). This

Table 1. Conversion of glucose to ethylene glycol and sorbitol on various metal oxides in the presence of Ru/C catalyst*

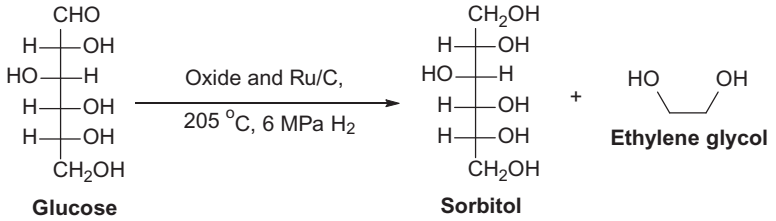

Entry	Oxide	Product yield (carbon %)		
		Sorbitol	Ethylene glycol	Others†
1	—	70.3	9.3	18.9
2	WO_3	9.2	59.4	23.3
3	Nb_2O_5	70.6	9.5	16.1
4	TiO_2	61.6	20.5	16.9
5	ZrO_2	58.8	19.9	18.1
6	Al_2O_3	54.5	23.6	20.6
7	V_2O_5	3.1	14.6	13.7
8	MnO_2	1.6	4.4	9.2
9	MoO_3	5.3	10.0	17.8
10‡	WO_3/Al_2O_3	8.8	62.6	21.7
11‡	WO_3/TiO_2	9.0	58.8	23.1
12‡	WO_3/SiO_2	7.9	66.8	21.6

*Reactions were performed with 0.50 mmol of glucose, 0.02 g of 3 wt % Ru/C, 1.0 g of oxide and 40 mL of H_2O. Glucose conversions were 100%.
†Other products include mannitol, pentitols, tetritols, propylene glycol, and glycerol (*SI Appendix*, Table S1).
‡WO_3 surface densities were 7.2, 7.0, and 6.8 W/nm^2 on Al_2O_3, TiO_2, and SiO_2, respectively; 0.016 g of WO_3 loading in reaction.

is due to the stoichiometric reduction of V_2O_5, MnO_2, and MoO_3 into VO_2, Mn_3O_4, and MoO_2 (*SI Appendix*, Fig. S1) by glucose under the reaction condition that competed with the glucose reaction on Ru, leading to its inefficient hydrogenation and low carbon balance. Supported WO_3 catalysts showed improved activities as a result of the increased accessibility of the WO_3 sites (Table 1, entries 10–12). When WO_3 crystallites were supported on Al_2O_3, TiO_2, and SiO_2 with a surface density around 7 W/nm^2 (*SI Appendix*, Fig. S2), the ethylene glycol yield reached 62.6, 58.8, and 66.8%, respectively, even using only 16 mg of WO_3 (Table 1, entries 10–12). These results show that WO_3 is different from the other metal oxides and can efficiently catalyze the C-C cleavage in the conversion of glucose to ethylene glycol. Such a distinct property of WO_3 is clearly not due to its distinct surface acidity and reducibility, as discussed below.

Besides glucose, other sugars of different type (aldose or ketose), carbon number, and chirality were also examined on WO_3 with an Ru/C catalyst. As shown in Table 2, mannose, the C2 epimer of glucose, was converted to ethylene glycol with a similar yield of 54.2% (Table 2, entry 2). However, conversion of ketohexoses, i.e., fructose and sorbose, yielded 47.9 and 47.7% propylene glycol as the major product, and ethylene glycol yields were only 15.7 and 12.9%, respectively (Table 2, entries 3 and 4). Aldopentoses, including xylose, ribose, arabinose, and lyxose, reacted to form nearly an equimolar mixture of ethylene glycol (25.8 to 32.1%) and propylene glycol (29.0 to 35.5%) (Table 2, entries 5–8). Aldotetroses (erythrose and threose), representing the typical chiralities of sugars, afforded similar ethylene glycol yields of 47.9 and 49.3% (Table 2, entries 9 and 10). These results reveal the characteristics of this sugar reaction on WO_3: all sugars are reactive, and the C-C bond cleavage selectively takes place at the β-position to the carbonyl group, independent of their carbon number, type (aldoses or ketoses), and chirality.

An essential requirement of the α-hydroxyl group for the C-C bond cleavage in sugar molecules is a nonclassical retro-aldol condensation mechanism. The above characteristics of the C-C bond cleavage on WO_3 resemble those of the typical retro-aldol reaction. In general, the retro-aldol condensation happens for β-hydroxyl aldehydes and ketones. Considering that each noncarbonyl carbon atom in a sugar molecule bears a hydroxyl group, we next examine the role of the individual

Table 2. Conversion of sugars to ethylene glycol and propylene glycol on WO_3 and Ru/C*

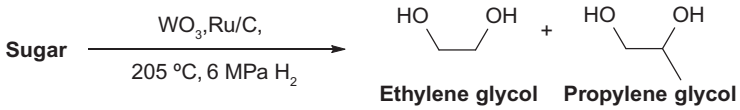

Entry	Sugar	Product yield (carbon %)		
		Ethylene glycol	Propylene glycol	Others†
1	Glucose	59.4	14.1	18.4†
2	Mannose	54.2	11.3	29.6†
3	Fructose	15.7	47.9	38.9†
4	L-sorbose	12.9	47.7	29.6†
5	Xylose	32.1	35.5	30.8‡
6	Ribose	25.8	29.0	28.2‡
7	Arabinose	28.7	30.2	27.7‡
8	Lyxose	29.5	32.2	27.1‡
9	Erythrose	47.9	11.0	32.2§
10	Threose	49.3	10.4	29.5§

*Reactions were performed with 0.50 mmol of sugar, 0.02 g of 3 wt % Ru/C, 1.0 g of WO_3 and 40 mL of H_2O. Sugar conversions were 100%.
†Hexitols, pentitols, tetritols, and glycerol.
‡Pentitols, tetritols, and glycerol.
§Tetritols and glycerol (*SI Appendix*, Table S2).

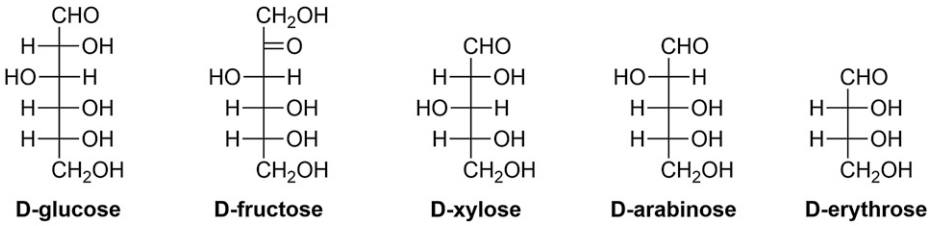

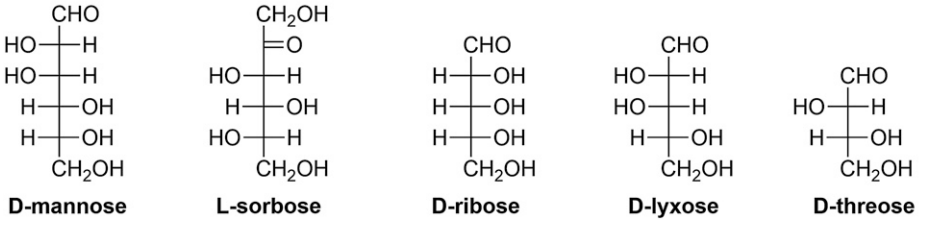

Table 3. Reaction of glucose and deoxysugars on Ru/C and WO_3

Entry	Reactant	Major product (yield %)		
1	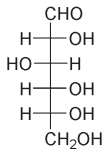 (Glucose)	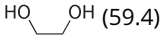 (59.4)		
2	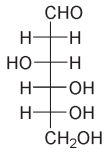 (2-deoxy-glucose)	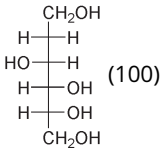 (100) (2-deoxy-sorbitol)		
3	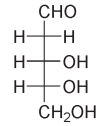 (2-deoxy-ribose)	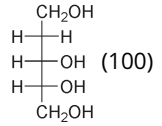 (100) (2-deoxy-ribitol)		
4	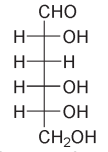 (3-deoxy-glucose)	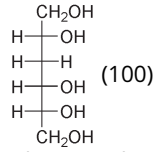 (100) (3-deoxy-sorbitol)		
5	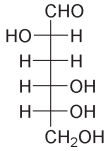 (3-deoxy-mannose)	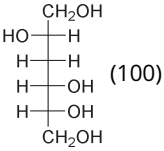 (100) (3-deoxy-mannitol)		
6	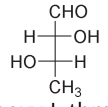 (4-deoxy-L-threose)	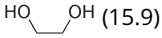 (15.9)	 (13.7) (4-deoxy-L-threitol)	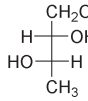 (52.6)
7	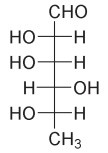 (6-deoxy-L-mannose)		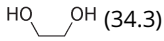 (34.3) 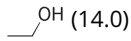 (14.0)	
8	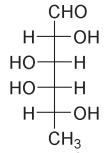 (6-deoxy-galactose)		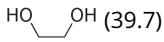 (39.7) 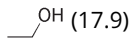 (17.9)	

Reactions were performed with 0.50 mmol of sugar, 0.02 g of 3 wt % Ru/C, 1.0 g of WO_3, 40 mL of H_2O, 6 MPa of H_2 at 205 °C for 10 min. Conversions were 100%.

hydroxyl groups in the reaction by comparing the activity of different deoxysugars. As shown in Table 3, the reactions of 2-deoxy-glucose and 2-deoxy-ribose on WO_3 and Ru/C yielded neither ethylene glycol nor propylene glycol but only their corresponding hydrogenation products, i.e., 100% 2-deoxy-sorbitol and 2-deoxy-ribitol, respectively (Table 3, entries 2 and 3). The reactions of 3-dexoy-glucose and 3-deoxy-mannose also produced only 3-deoxy-sorbitol and 3-deoxy-mannitol, respectively (Table 3, entries 4 and 5). Therefore, both α- and β-hydroxyl groups are required for selective cleavage of C-C bonds at the β-position to the carbonyl group in sugars. To further understand such a structural requirement, we next used 4- and 6-deoxysugars as substrates (Table 3, entries 6–8). The reaction of 4-deoxy-L-threose produced ethylene glycol and ethanol at an essentially equal amount (15.9 and 13.7%) with 4-deoxy-L-threitol (52.6%). Rhamnose (6-deoxy-L-mannose) and fucose (6-deoxy-galactose), both yielded ethylene

glycol and ethanol with a molar ratio of ~2:1. This ratio is caused by the C-C bond cleavage of 6-deoxy-hexose to form one glycolaldehyde molecule and one 4-dexoy-tetrose molecule, of which the latter underwent further cleavage to form another glycolaldehyde molecule and one acetaldehyde molecule. Clearly, 4-deoxy-tetrose, as either the starting reactant or the intermediate, can undergo the selective C-C bond cleavage on WO_3, indicating that the γ-hydroxyl group is not necessarily involved in the reaction. This is also supported by the higher reaction rate of 4-deoxy-tetrose than that of the normal tetrose (i.e., erythrose) (*SI Appendix*, Fig. S3). This rate difference may be due to their different conformation in the aqueous solution: the normal tetrose is usually present in a cyclic structure (erythrofuranose), where its carbonyl group is in the form of hemiacetal, whereas the 4-deoxy-tetrose is in the chain conformation, where its carbonyl group is exposed and thus more reactive. Taken together, these results reveal that the γ-hydroxyl group in sugars is not necessarily required for the β-C-C bond cleavage but that the α- and β-hydroxyl groups are unequivocally indispensable for this reaction.

Mechanism of C-C Bond Cleavage Involving an Ethenediol Intermediate. To further understand the sugar reaction on WO_3, we closely compared the reaction kinetics of glucose and erythrose on WO_3 in the absence of Ru/C and H_2. The evolution of the products with time in the glucose reaction is shown in Fig. 1*A*. Mannose, the C2 epimer of glucose, appeared immediately after the reaction, and its yield increased rapidly to ~10% in 10 min and then declined gradually. Two tetroses, erythrose and threose, were also formed from the beginning of the reaction. Both quickly reached their maximum yield of ~1.3% and slowly declined thereafter. Glycolaldehyde showed a monotonic increase, behaving as an end product. From the slopes of the evolution curves of glycolaldehyde, erythrose, threose, and mannose at the initial reaction time, their initial formation rates were extracted. The rate of glycolaldehyde (27 μmol/g_{WO3}/min) was nearly equal to the sum of the rates of erythrose (13 μmol/g_{WO3}/min) and threose (11 μmol/g_{WO3}/min). This substantiates that the C-C bond cleavage of glucose takes place at the β-position to the carbonyl group to form equimolar tetroses and glycolaldehyde. The initial formation rate of

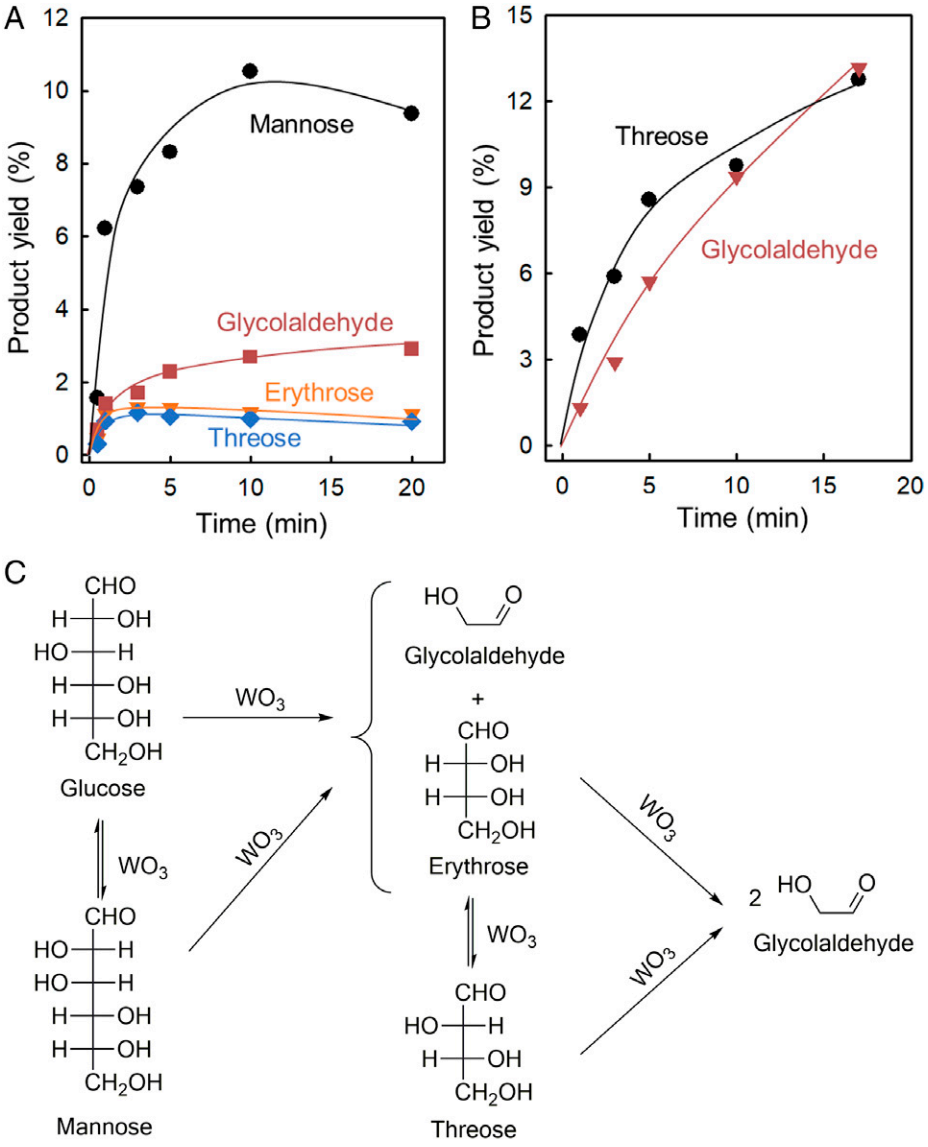

Fig. 1. Reaction of glucose (*A*) and erythrose (*B*) on WO_3 as a function of reaction time. (*C*) Reaction pathway of glucose on WO_3. Reaction conditions: 0.18 mmol of glucose or erythrose, 0.40 g of WO_3 for the glucose reaction, 0.04 g of WO_3 for the erythrose reaction, 165 °C, 15 mL of H_2O, 6 MPa of N_2.

mannose (45 μmol/g_{WO3}/min) was larger than that of glycolaldehyde, indicating faster C2 epimerization of glucose than its C-C bond cleavage. These results demonstrate the bifunctional role of WO_3 for the C2 epimerization and C-C bond cleavage in the sugar reactions. The erythrose reaction showed similar results (Fig. 1*B*). Its C2 epimer, threose, formed with an initial rate of 500 μmol/g_{WO3}/min, and the C-C bond cleavage product, glycolaldehyde, formed with a rate of 410 μmol/g_{WO3}/min. From these results, we tentatively conclude that the reaction pathways of glucose on WO_3, as depicted in Fig. 1*C*, include the primary epimerization of glucose at the C2 position to mannose and the C-C bond cleavage at the β-position to its carbonyl group to glycolaldehyde and erythrose, followed by the secondary reactions of the mannose and erythrose intermediates to ultimately form glycolaldehyde. The C2-epimerization step was confirmed to be reversible by a separate reaction of mannose on WO_3, showing the formation of glucose in a 28.7% yield after 30 min at 165 °C.

To further confirm the reaction mechanism, three different ^{13}C-labeled glucoses were used as reactants to track the isotope distributions in the products. Fig. 2 shows the ^{13}C-NMR spectra of the products in the reactions of [1-^{13}C]-glucose, [2-^{13}C]-glucose, and [6-^{13}C]-glucose on WO_3. For [1-^{13}C]-glucose, the two strong signals at 92.9 and 96.7 ppm (Fig. 2*A*) are the characteristic chemical shifts of the C1 carbon of its carbonyl group, present in the α- and β-glucopyranose forms, respectively (46, 47). After the reaction of [1-^{13}C]-glucose, two new pairs of signals appeared in the ^{13}C-NMR spectrum (Fig. 2*A*). The pair at 71.5 and 72.0 ppm is assigned to the chemical shifts of the C2 carbon atoms of α- and β-mannopyranose ([2-^{13}C]-mannose), respectively (46, 47), indicating the epimerization of glucose to mannose via the C1-C2 carbon skeleton rearrangement. The other pair at 89.8 and 64.6 ppm corresponds to the chemical shifts of the C1 and C2 carbon atoms of glycolaldehyde ([1-^{13}C]-glycolaldehyde and [2-^{13}C]-glycolaldehyde), respectively (48). [2-^{13}C]-glucose had two strong signals at chemical shifts of 72.3 and 74.9 ppm (Fig. 2*B*), corresponding to the C2 carbon of its α- and β-glucopyranose forms. After its reaction, the produced mannose was labeled by ^{13}C at its C1 position ([1-^{13}C]-mannose), as evidenced by the signals at 94.8 ppm (α-mannopyranose) and 94.4 ppm (β-mannopyranose) (46, 47), and both ^{13}C1-labeled (89.8 ppm) and ^{13}C2-labeled (64.6 ppm)

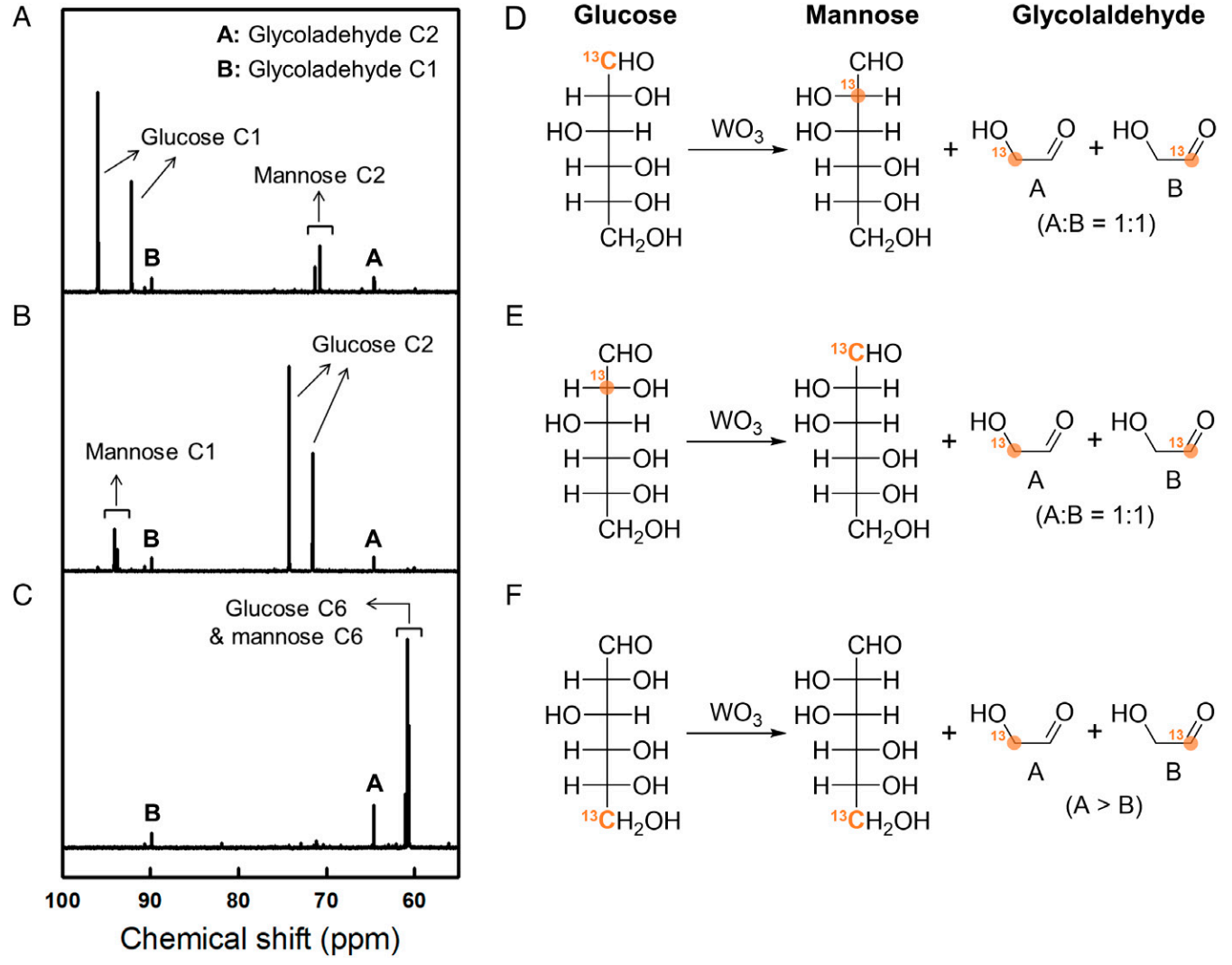

Fig. 2. ^{13}C-NMR spectra of the product solutions of (*A*) [1-^{13}C]-glucose, (*B*) [2-^{13}C]-glucose, and (*C*) [6-^{13}C]-glucose reacting on WO_3. (*D–F*) Schematic illustration of the ^{13}C labeling in reactants and products. Orange indicates the ^{13}C-labeled carbon. Reaction conditions: 50 μmol of glucose, 0.40 g of WO_3, 15 mL of H_2O, 165 °C, 30 min, 6 MPa of N_2. Only signals of ^{13}C-labeled carbons are visible, because unlabeled carbons rich in ^{12}C (98.9% natural abundance) are not detectable on NMR. Each carbon atom in glucose or mannose shows a pair of signals because of the coexistence of α- and β-glucopyranose or α- and β-mannopyranose forms in an aqueous phase.

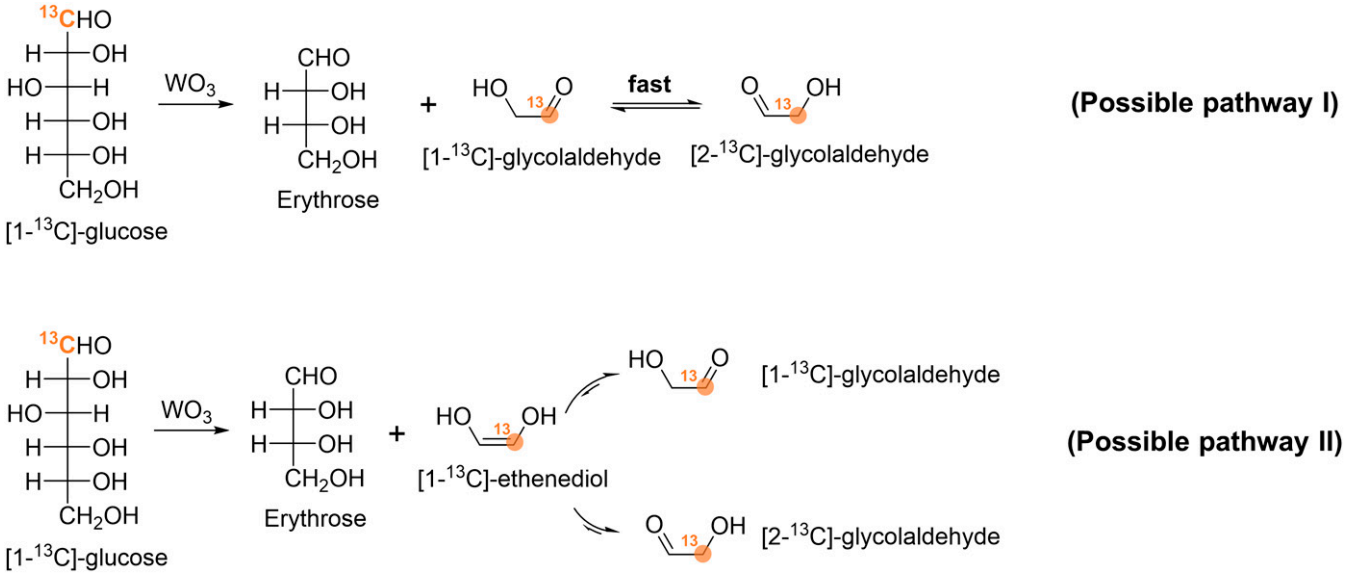

Scheme 1. Plausible pathways to form equimolar [1-^{13}C]-glycolaldehyde and [2-^{13}C]-glycolaldehyde from the [1-^{13}C]-glucose reaction. Orange indicates the ^{13}C-labeled carbon.

glycoladehydes ([1-^{13}C]-glycolaldehyde and [2-^{13}C]-glycolaldehyde) existed (Fig. 2*B*). Noticeably, in both reactions of [1-^{13}C]-glucose and [2-^{13}C]-glucose, the produced glycolaldehyde showed the same pattern of ^{13}C-labeling, indicating that equal amounts of [1-^{13}C]-glycolaldehyde and [2-^{13}C]-glycolaldehyde were formed on WO_3 (Fig. 2 *D* and *E*). Such equal probability can be explained by two possible reaction pathways (Scheme 1). Taking the [1-^{13}C]-glucose reaction for example, it is possible to produce equimolar [1-^{13}C]-glycolaldehyde and [2-^{13}C]-glycolaldehyde if the tautomerization between [1-^{13}C]-glycolaldehyde and [2-^{13}C]-glycolaldehyde is very fast that facilitates the scrambling of the ^{13}C-labeling in the glycolaldehyde molecules (Scheme 1, pathway I), or glycolaldehyde is formed via the [1-^{13}C]-ethenediol intermediate that equally turns into [1-^{13}C]-glycolaldehyde and [2-^{13}C]-glycolaldehyde (Scheme 1, pathway II).

To verify which of the two pathways (I and II) actually occurs in the reaction, [6-^{13}C]-glucose was examined in the reaction. If the reaction followed pathway I, as discussed above, equimolar [1-^{13}C]-glycolaldehyde and [2-^{13}C]-glycolaldehyde would be formed, which is indeed not consistent with the reaction results, as shown in Fig. 2*C*. The unconverted [6-^{13}C]-glucose showed two signals at 61.4 and 61.6 ppm (Fig. 2*C*), assigned to the C6 carbon of the α- and β-glucopyranose forms (46, 47). The produced mannose was also labeled at C6, shown by the chemical shift at 61.8 ppm (Fig. 2*C*) (46, 47). For glycolaldehyde, the signal of the C2 carbon (64.6 ppm) is much stronger than that of the C1 carbon (89.8 ppm) (Fig. 2*C*), in contrast to the observation in the reactions of [1-^{13}C]-glucose and [2-^{13}C]-glucose (Fig. 2 *A* and *B*). The dominant presence of [2-^{13}C]-glycolaldehyde over [1-^{13}C]-glycolaldehyde in the [6-^{13}C]-glucose reaction shows that the tautomerization between the glyceraldehyde molecules is essentially slow (Fig. 2*F*), from which pathway I can be excluded.

Based on the above results, we conclude the reaction pathway of the C2 epimerization and C-C bond cleavage of glucose on WO_3 is as shown in Scheme 2, exemplified by the reaction of [1,6-$^{13}C_2$]-glucose. The C2 epimerization of [1,6-$^{13}C_2$]-glucose forms [2,6-$^{13}C_2$]-mannose via the C1-C2 carbon skeleton rearrangement. The C-C bond cleavage of [1,6-$^{13}C_2$]-glucose occurs selectively at its β-position, primarily producing the equal molar amounts of [1-^{13}C]-ethenediol and [4-^{13}C]-erythrose, of which the former intermediate rapidly tautomerizes equiprobably into [1-^{13}C]-glycolaldehyde and [2-^{13}C]-glycolaldehyde while the latter undergoes further C-C bond cleavage into 1,2-ethenediol and [2-^{13}C]-glycolaldehyde.

Structure of Sugar Molecules Bonding to the WO_3 Surface. The C2 epimerization of glucose into mannose has been proposed in the aqueous solution of molybdic acid, involving a sugar-bimolybdate complex (*SI Appendix*, Scheme S2) (49). This reaction is characteristic of the C1-C2 shift in the carbon skeleton and involvement of the α- and β-hydroxyl groups.

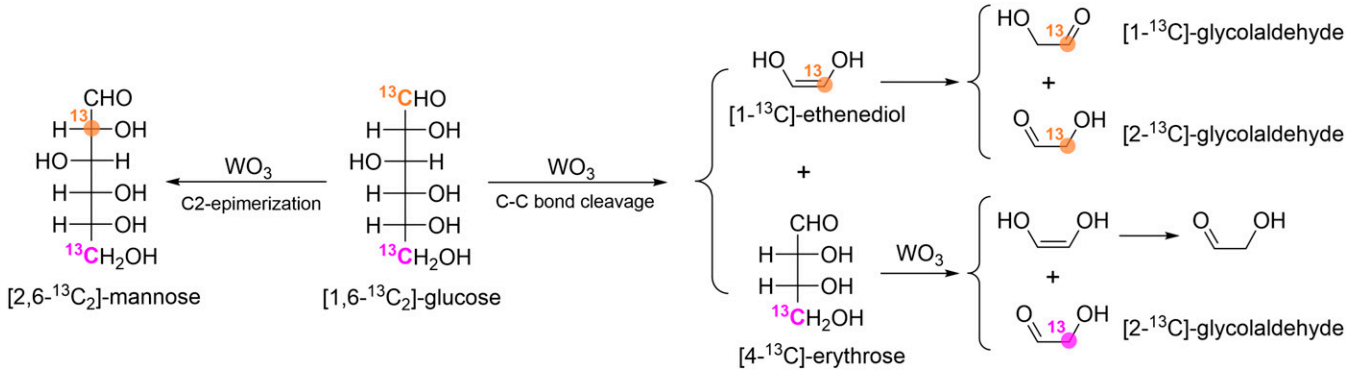

Scheme 2. Reaction pathways of [1,6-$^{13}C_2$]-glucose on WO_3. Orange and pink trace the ^{13}C1 and ^{13}C6 of glucose in the intermediates and final products.

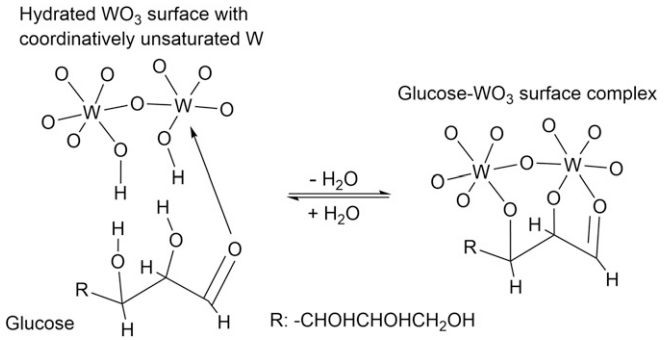

Scheme 3. Proposed structure of glucose adsorbed on the WO_3 surface.

Since the glucose reaction on WO_3 has the same characteristics, we propose that the sugar reaction proceeds via a sugar-bitungstate complex on the WO_3 surface (Scheme 3).

In order to characterize the glucose-WO_3 surface complex, we collected solid-state ^{13}C-NMR (Fig. 3) and Ultraviolet-visible (UV-vis) spectra (Fig. 4) for glucose adsorbed on WO_3 (glucose/WO_3). Glucose in the aqueous solution possesses 12 NMR signals (Fig. 3*A*): α-glucopyranose C1 (92.9 ppm), C2 (72.3 ppm), C3 (73.6 ppm), C4 (70.5 ppm), C5 (72.2 ppm), and C6 (61.4 ppm) and β-glucopyranose C1 (96.7 ppm), C2 (74.9 ppm), C3 (76.5 ppm), C4 (70.5 ppm), C5 (76.7 ppm), and C6 (61.6 ppm) (46, 47). Upon adsorption on WO_3 at 25 °C, these signals remained identical chemical shifts, but they showed line broadening (Fig. 3*B*) due to the strong anisotropic effect in solid-state NMR. After thermal activation at 120 °C for 1 h, several new signals appeared around 105 and 83 ppm (Fig. 3*C*). These changes are attributed to the new species formed upon the interaction between glucose and WO_3, because they were not observed when WO_3 was replaced by SiO_2 after identical thermal treatment (glucose/SiO_2, *SI Appendix*, Fig. S4). In order to assign these new ^{13}C-NMR signals, we compared the ^{13}C-NMR spectra of [1-^{13}C]-glucose, [2-^{13}C]-glucose, and [3-^{13}C]-glucose adsorbed on WO_3. For [1-^{13}C]-glucose on WO_3, a broad signal around 105 ppm appeared (Fig. 3*D*), which belongs to the glucose C1 carbon, shifted from positions at 92 ppm (α-glucopyranose) and 97 ppm (β-glucopyranose). This shift is due to the deshielding effect on the formation of the W-O-C bond, as reported for the sugar-bitungstate complexes in aqueous solutions (50–53). The same phenomenon was also observed for [2-^{13}C]-glucose and [3-^{13}C]-glucose adsorbed on WO_3, which showed a shift of the glucose C2 peak from 72 ppm (α-glucopyranose) and 75 ppm (β-glucopyranose) to ∼83 ppm (Fig. 3*E*) and the glucose C3 peak from 74 ppm (α-glucopyranose) and 77 ppm (β-glucopyranose) to ∼86 ppm (Fig. 3*F*). The shifts of about 10 ppm for the signals of both glucose C2 and C3 carbons indicate the formation of W-O-C bonds with C2 and C3 carbons. Based on these results, we propose that glucose binds with the WO_3 surface at its C1, C2, and C3 positions, forming the glucose-tungstate tridentate complex (Scheme 3), which is consistent with the observed essential involvement of both α- and β-hydroxyl groups, together with the carbonyl group, in the glucose reaction (Table 3).

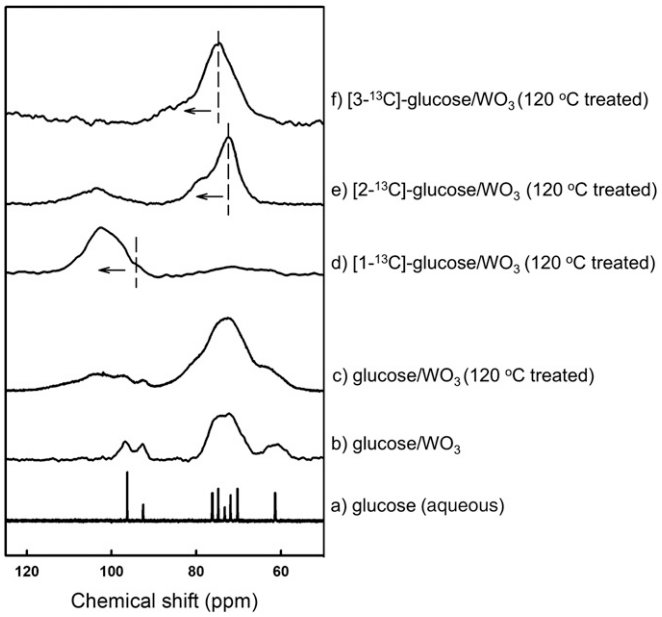

Fig. 3. ^{13}C-NMR spectra of glucose after different treatments: (*A*) aqueous glucose in D_2O; (*B*) glucose adsorbed on WO_3; and (*C*–*F*) unlabeled glucose, [1-^{13}C]-glucose, [2-^{13}C]-glucose, and [3-^{13}C]-glucose adsorbed on WO_3 and thermal treated at 120 °C for 1 h. All spectra were collected at 25 °C. The arrow and dashed lines indicate the chemical shifts of the (*D*) C1 carbon, (*E*) C2 carbon, and (*F*) C3 carbon of glucose.

The UV-vis spectra further confirm the interaction between glucose and WO_3. Fig. 4*A* shows the UV-vis spectra of glucose adsorbed on WO_3 (glucose/WO_3) before and after thermal treatment at 120 °C under a N_2 flow for 1 h. Before the treatment, the spectra had an absorption peak of WO_3 at 360 nm (54). After the treatment, the absorbance above 450 nm upshifted by about 0.15, with a concurrent change in the color of WO_3 from yellow to light green, indicative of the formation of new discrete bands in the forbidden band gap of WO_3. This phenomenon is known for partly reduced WO_3, i.e., $W^{(6-\delta)+}O_{3-x}$ (54). When using sorbitol instead of glucose, neither the shift of the UV-vis band nor the color change of WO_3 was observed (Fig. 4*B*). Therefore, it is concluded that the carbonyl group of glucose is critical for the observed partial reduction of the W^{6+} sites at the WO_3 surface. In combination with the results from the ^{13}C-NMR characterization (Fig. 3), showing the formation of the W-O-C1 bond (C1 refers to the glucose C1 carbon) between the adsorbed glucose molecule and the WO_3 surface, we surmise that a coordinatively unsaturated surface W^{6+} site as a Lewis acid site binds with the O atom of the C=O group in glucose, forming a new W-O=C bond to polarize the C=O bond (Scheme 3). Subsequently, two adjacent hydroxyl groups on the WO_3 surface interact with the α- and β-hydroxyl groups of glucose to form the W-O-C2 and W-O-C3 bonds, leading to the formation of the glucose-WO_3 tridentate complex. This surface complex is reactive and undergoes epimerization via the C1-C2 carbon skeleton rearrangement to form mannose and the C-C bond cleavage via the retro-aldol condensation to form equimolar tetrose and 1,2-ethenediol intermediates, as depicted in Scheme 4. Clearly, this mechanism for C-C bond cleavage is different from the classical retro-aldol condensation that requires the participation of only the β-hydroxyl group, rather than both α- and β-hydroxyl groups.

Theoretical Assessment of Sugar Reaction on WO_3. Periodical density functional theory (DFT) calculations were further employed to substantiate the aforementioned surface intermediate and reaction mechanism for C-C cleavage of sugar on the WO_3 surface. L-threose, a C_4 sugar with C1-C3 moieties identical to those of glucose, was chosen here as a model reactant, and a hydroxylated (001) surface of monoclinic WO_3 was constructed to represent the working WO_3 catalyst under the hydrothermal condition (details shown in *Materials and Methods*). For comparison, the reaction of 2-deoxy-L-threose was also simulated to verify the role of the α-OH group. As shown in Fig. 5,

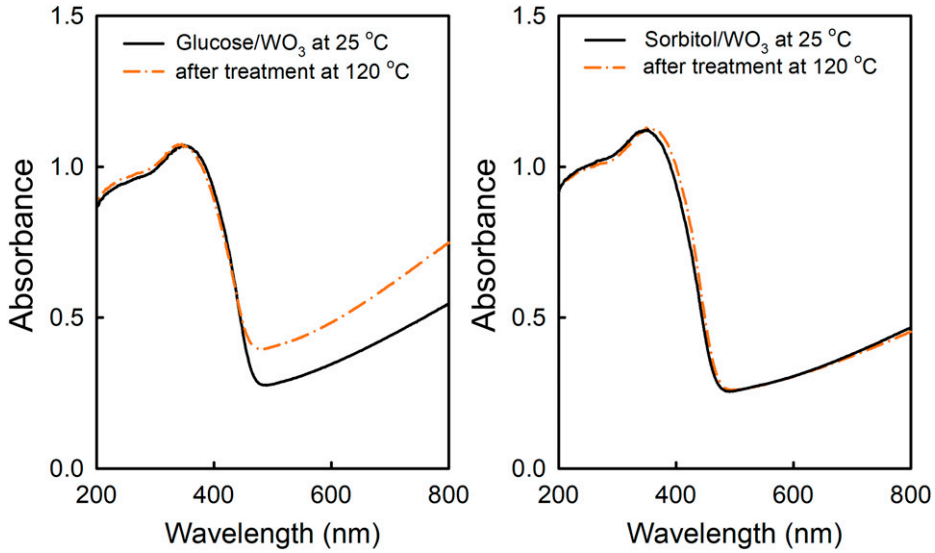

Fig. 4. UV-vis spectra of (*A*) glucose and (*B*) sorbitol loaded on the WO_3 surface before and after thermal treatment at 120 °C in a N_2 flow. Spectra were recorded at 25 °C.

dehydration of L-threose on the WO_3 (001) surface formed a tridentate complex, in which the C=O group was bound to an oxygen vacancy and the α- and β-hydroxyl O atoms were coordinated with two neighboring W sites. The C-C bond cleavage of this intermediate was almost energy neutral (−0.01 eV) with a low activation barrier of 0.53 eV, producing a surface-bound 1,2-ethenediol intermediate and a glycolaldehyde intermediate. In contrast, the C-C cleavage of 2-deoxy-L-threose on the WO_3 surface was endothermic (0.20 eV) and showed a higher activation barrier of 0.62 eV. These differences indicate that the presence of α-OH in L-threose makes the C-C bond cleavage both thermodynamically and kinetically more favorable, reflecting the stabilization of the transition state for the C-C cleavage and the surface-bound ethenediol species conferred by the strong interaction of the α-OH group with the surface W site. These DFT results are consistent with the reaction mechanism involving the surface tridentate complex and ethenediol intermediates, as depicted in Scheme 4, and unveil the critical role of α-OH in determining the C-C bond cleavage activity on the WO_3 surface.

Potential Impact on Sugar Utilization in Future Biomass Refinery. As discussed above, the formation of the glucose-WO_3 surface tridentate complex (Scheme 4) requires at least two adjacent tungsten atoms (i.e., W-O-W sites) on the catalysts. This is consistent with our previous finding that the catalytic sites for the C-C cleavage are based on the aggregated WO_3 structures while highly dispersed WO_3 species are not active at all (13). If this mechanism is true, any tungsten compounds containing the W-O-W sites will be catalytically active for this sugar reaction, as indeed observed in the following tests. Table 4 compiles the reaction of glucose catalyzed by several representative W-based compounds. Ammonium paratungstate $(NH_4)_{10}[H_2W_{12}O_{42}]$ is a soluble salt in water containing W-O-W bonds, which catalyzed the reaction of glucose to

Table 4. Conversion of glucose to ethylene glycol and sorbitol on various W-based catalysts*

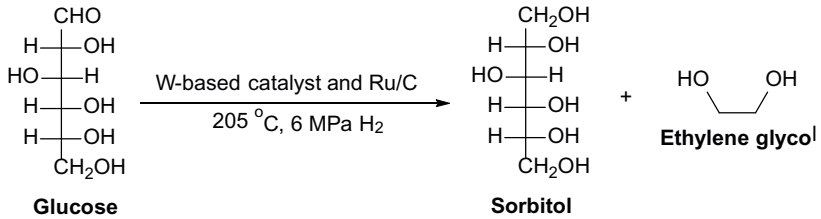

Entry	W-based catalyst	Product yield (carbon %)		
		Sorbitol	Ethylene glycol	Others†
1	—	70.3	9.3	18.9
2	$(NH_4)_{10}[H_2W_{12}O_{42}]$	8.1	60.7	10.9
3	$Cs_{2.5}H_{0.5}PW_{12}O_{40}$	42.6 (16.0)‡	30.6 (52.3)‡	21.0 (21.7)‡
4	$H_{0.23}WO_3$	32.1	36.0	16.9
5	WO_2	7.1	61.3	28.7
6	W	5.9	59.6	28.6
7	W_2C	12.3	57.3	23.8

*Reactions were performed with 0.50 mmol of glucose, 0.02 g of 3 wt % Ru/C and 1.0 g of W-based catalyst in 40 mL of H_2O, except soluble $(NH_4)_{10}[H_2W_{12}O_{42}]$ of 0.1 g. Glucose covnersions were 100%.

†Other products include mannitol, pentitols, tetritols, propylene glycol, and glycerol (*SI Appendix*, Table S3).

‡2.0 g of $Cs_{2.5}H_{0.5}PW_{12}O_{40}$ loaded for values in parentheses.

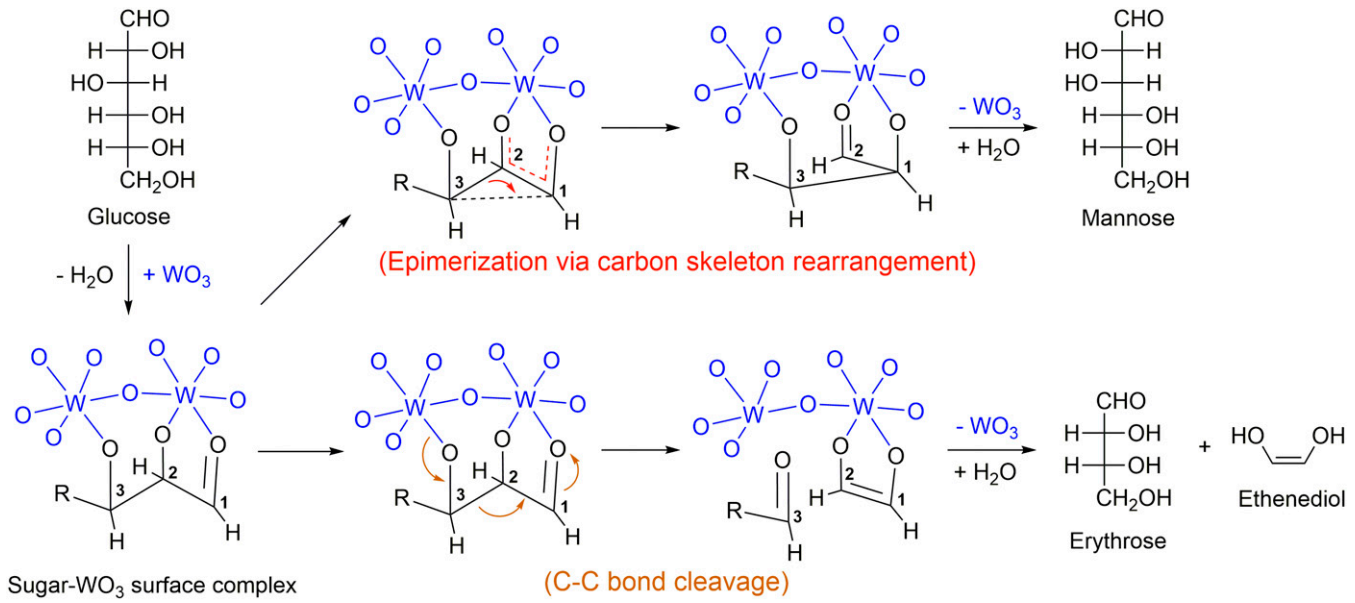

Scheme 4. Proposed mechanism for C2 epimerization and C-C bond cleavage of glucose on WO_3.

yield 60.7% ethylene glycol in the presence of Ru/C and H_2 (Table 4, entry 2). The polyoxometalate $Cs_{2.5}H_{0.5}PW_{12}O_{40}$, hydrogen tungsten bronze $H_{0.23}WO_3$, and WO_2 also contain the W-O-W structure and afforded 30.6, 36.0, and 61.3% yields of ethylene glycol, respectively (Table 4, entries 3–5). The lower yields of ethylene glycol for the former two samples are due to their lower surface areas, as shown by the result that increasing the loading, e.g., $Cs_{2.5}H_{0.5}PW_{12}O_{40}$, effectively enhanced the yield to 52.3% (Table 4, entry 3, in parentheses). Even W metal and W_2C are active in the glucose reaction to ethylene glycol with a yield of 59.6 and 57.3%, respectively, because the W-O-W sites are generated by in situ oxidation under the hydrothermal conditions during the glucose reaction (13). The reported catalysts effective for this reaction in literature, including tungstic acid (H_2WO_4) (12), hydrogen tungsten bronze (H_xWO_3) (15), metatungstate salts (28, 30), polyheterogeneous acids ($H_3PW_{12}O_{40}$ and $H_4SiW_{12}O_{40}$) (15, 30, 34), and metal-organic frameworks containing phosphotungstic acid moieties (33), despite of their different compositions and structures, all possess the W-O-W sites. Taken together, these results

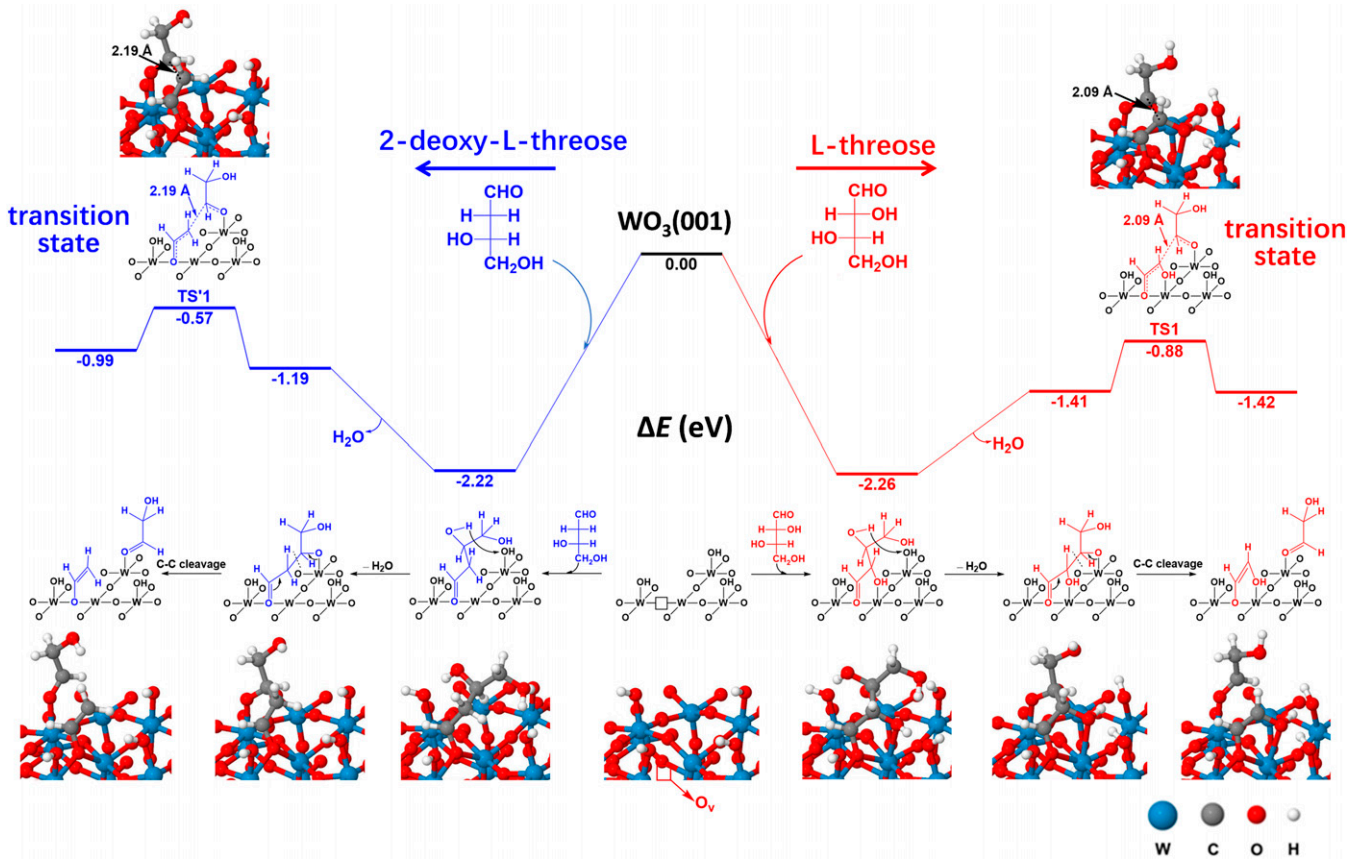

Fig. 5. Energy profiles calculated by DFT for the reactions of L-threose (red) and 2-deoxy-L-threose (blue) on the (001) surface of m-WO_3.

clearly demonstrate that this mechanism is applicable to different W-based catalysts and sugar reactants.

Conclusions

WO_3 crystallites efficiently catalyze selective cleavage of C-C bonds for all $C_{4–6}$ sugars, irrespective of their carbon numbers, types (aldoses and ketoses), and chiralities, to $C_{2,3}$ oxygenate intermediates (glycolaldehyde and glyceraldehyde), which then convert to ethylene glycol and propylene glycol in the presence of Ru/C and H_2. The sugar molecule adsorbs on the WO_3 surface to form a tridentate complex via coordination of its carbonyl group and α- and β-hydroxyl groups with two adjacent tungsten atoms (i.e., W-O-W sites). This surface tridentate complex is the critical intermediate for the subsequent C-C bond cleavage that occurs primarily at the β-position to the carbonyl group to form the $C_{2,3}$ intermediates, for example, 1,2-ethenediol in the glucose reaction. The essential requirement for both α- and β-hydroxyl groups is clearly different from the classical retro-aldol condensation that requires the presence of only the β-hydroxyl group. This reaction mechanism deciphers the critical W-O-W structures as the catalytic active sites on all hitherto developed tungsten-based catalysts to selectively break the C-C bonds of sugars, which will be beneficial to the rational design of more efficient catalysts. The generic activity of this reaction for all sugar molecules of different compositions and structures enables the facile conversion of the mixed sugar feedstocks, in one step without separation and purification, to the same $C_2H_4O_2$ and $C_3H_6O_3$ intermediates, which will boost the practicability of such $C_{2,3}$ intermediates as the platform molecules for producing various chemicals from cellulose and other sugar-based biomass.

Materials and Methods

Materials. WO_3 Analytical reagent grade (AR) was purchased from Beijing Chemical Works. WO_2 (99.9%) and W_2C (99.5%) were from Alfa Aesar, and W (>99.8%) came from Sinopharm Chemical. D-glucose (AR), D-fructose (AR), and L-sorbose (AR) were from Beijing Chemical Works. D-mannose (99%), D-xylose (99%), D-arabinose (98%), D-ribose (99%), D-lyxose (99%), D-erythrose (70% syrup), 2-deoxy-D-glucose (98%), 2-deoxy-D-ribose (99%), D-fucose (6-deoxy-galactose, 99%), and L-rhamnose (6-deoxy-L-mannose, 99%) were all purchased from Alfa Aesar. D-threose (60% syrup), glycolaldehyde, and DL-glyceraldehyde (95%) were purchased from Sigma-Aldrich. ^{13}C-labeled materials, [1-^{13}C]-D-glucose (99%), [2-^{13}C]-D-glucose (99%), [3-^{13}C]-D-glucose (99%), and [6-^{13}C]-D-glucose (99%) were purchased from Sigma-Aldrich. Supported WO_3 catalysts (WO_3/Al_2O_3, WO_3/TiO_2, and WO_3/SiO_2) were prepared by wetness impregnation of corresponding supports with aqueous solutions of ammonium paratungstate (AR, Sinopharm Chemical), followed by drying at 120 °C and calcination at 500 °C in flowing air.

4-deoxy-L-threose, 3-deoxy-D-glucose, and 3-deoxy-D-mannose were prepared using the reported methods (55, 56). 4-deoxy-L-threose was prepared by oxidation of L-rhamnose with lead tetraacetate $Pd(OAc)_4$, followed by acid hydrolysis. In brief, 2 mL of water containing 2.5 g of L-rhamnose was mixed with 250 mL of water containing 15 g of $Pd(OAc)_4$ with stirring at room temperature for 40 min. Afterward, 6 g of anhydrous oxalic acid was added to precipitate the lead oxalate. After filtration and evaporation, the syrup was dissolved in 100 mL of 0.1% H_2SO_4 and kept at 37 °C for 6 h. Then the solution was adjusted to pH > 5.5 by treatment with (HCO_3^-) ion-exchange resin. After removal of the resin, the aqueous solution of 4-deoxy-L-threose was obtained.

3-deoxy-D-glucose and 3-deoxy-D-mannose were prepared by condensation of 2-deoxy-D-ribose with nitromethane, giving 1-nitro-1,3-dideoxy-hexitol, which turns into a mixture of 3-deoxy-D-glucose and 3-deoxy-D-mannose via a Nef reaction. In brief, at 0 °C, 20 mL of anhydrous methanol solution containing 1 g of sodium methoxide was added dropwise to 10 mL of anhydrous methanol suspension containing 2 g of 2-deoxy-D-ribose and 2.4 mL of nitromethane. After reaction at 5 °C for 25 h, the solution was diluted with 30 mL of cold water and then passed through (H^+) ion-exchange resin. Then, 23 mL of 2 mol/L NaOH solution was added dropwise to the obtained eluate at 0 °C. Afterward, the solution was kept to −20 °C and 20 mL of 40% H_2SO_4 was added dropwise into the solution under vigorous agitation. Afterward, the solution was neutralized at 0 °C by adding an aqueous NaOH solution. After filtration, the solution was treated with (H^+) ion-exchange resin and then evaporated to a syrup. The syrup is a mixture of 3-deoxy-D-glucose and 3-deoxy-D-mannose. The two products were then separated chromatographically through a column filled with microcrystalline cellulose.

Catalytic Reactions of Sugars. Catalytic reactions of sugars were carried out in a stainless autoclave with pressurized H_2 or N_2 gas. Typically, a certain amount of reactants and catalysts, and also 40 mL of deionized water, were loaded in the autoclave and charged with 6 MPa of H_2. Under vigorous agitation, the autoclave was heated to 205 °C at a ramping rate of 10 °C/min. After a certain period, the reaction in the autoclave was quenched by cooling water and the temperature decreased to below 100 °C in 5 min. Solid catalysts were separated by filtration. The solid was washed with water three times, and the water was combined with the filtrates. In the filtrates, concentrations of sugar reactant and products were analyzed by High Performance Liquid Chromatography (HPLC) (Shimadzu LC 20A) equipped with an HPX-87C column from Bio-Rad Laboratories, Inc. The conversion of reactant was calculated by its concentration before and after the reaction. Product yield was calculated on a carbon basis, i.e., the mole of carbon atoms in a given product divided by the mole of carbon atoms in the reactant.

Characterization Methods. Aqueous ^{13}C-NMR spectra were recorded on a Bruker 500-MHz NMR spectrometer (500 MHz for ^{1}H-NMR and 125 MHz for ^{13}C-NMR) in D_2O/H_2O (1:3) solvent. ^{13}C (^{1}H decoupled) chemical shifts (δ) are reported in parts per million and are referenced to the α-glucopyranose C1 (δ92.9), C2 (δ72.3), and C6 (δ61.4).

Solid-state ^{13}C-NMR spectra were recorded on a Bruker 400-MHz solid-state NMR spectrometer at a ^{13}C resonance frequency of 100.6 MHz. A cross-polarization (CP)/total suppression of spin sidebands pulse program (5.8 μs) was applied. The CP contact time was 3 ms, with magic angle spinning at 5 kHz. The samples were pressed and sieved to 200 mesh and packed tightly in a cylindrical zirconia rotor with a diameter of 4 mm. For each spectrum, 300 to 3,000 scans were acquired depending on whether glucose was ^{13}C-labeled or not.

UV-vis spectra were collected on a PerkinElmer Lamda 650S UV-vis spectrometer equipped with a homemade UV-vis cell allowing control of temperature and N_2 gas flow. Sample powders (glucose or sorbitol adsorbed on WO_3) were pressed into self-standing wafers and then fixed into the cell facing the integral sphere through an optical-grade quartz window. Sample wafers were purged by a N_2 flow (25 mL/min) for 1 h at 25 °C, and then spectra were collected. Thereafter, the wafers were treated in a N_2 flow (25 mL/min) at 120 °C for 1 h. Upon the thermal treatment, the spectra were collected after cooling to 25 °C.

The solid samples (e.g., glucose adsorbed on WO_3) for solid-state ^{13}C-NMR and UV-vis spectra were prepared by wetness impregnation of WO_3 with the corresponding aqueous solutions of substrates, followed by drying in vacuum at 60 °C.

Computational Methods. Spin-polarized periodic DFT calculations were conducted using Vienna Ab initio Simulation Package (57–60) software with the projector augmented wave method (61). The generalized gradient approximation of the Perdew-Burke-Ernzerhof exchange-correlation functional (62) was employed to describe electron exchange and correlation, and van der Waals interactions between adsorbed species and the catalyst surface were adopted by means of Grimme's D3BJ approach, i.e. DFT-D3 scheme with zero-damping function given by Becke and Johnson (BJ-damping) (63). A plane-wave cutoff energy of 400 eV was applied for all calculations, in which the energy and residual forces were converged to 10^{-5} eV and 0.03 eV/Å, respectively.

The monoclinic WO_3 bulk structure was optimized through a 5 × 5 × 5 k-point grid based on a Monkhorst-Pack scheme. An oxygen-terminated WO_3 (001) surface with a p(2 × 2) superstructure was then constructed and used as the model catalyst in this study, considering this plane is the most stable surface for monoclinic WO_3 (64, 65). The dangling bonds of the terminated oxygen atoms were saturated by hydrogen atoms in order to simulate the hydroxylated WO_3 surfaces at the hydrothermal condition of sugar reaction. An oxygen vacancy was also introduced onto the WO_3 (001) surface (*SI Appendix*, Fig. S5) because of the reduced feature of WO_3 under the reaction conditions, as indicated by the UV-vis characterization (Fig. 4). A vacuum region of 30 Å was set to for the slab model to remove any long-range interactions among neighboring slabs. Brillouin zone sampling was conducted with a gamma point for structural

optimization, and 3 × 3 × 1 Monkhorst-Pack k-point meshes were then used to calculate the single point energy for all optimized structures. During the optimization, the atoms in the bottom three layers were fixed and the rest were allowed to relax freely. The transition states were located by climbing nudged elastic band (66) and dimer (67) methods.

Data, Materials, and Software Availability. All study data are included in the article and/or *SI Appendix*.

ACKNOWLEDGMENTS. This work was supported by the National Key Research and Development Program of China (Grant 2021YFA1501104), the National Natural Science Foundation of China (Grants 22032001, 21821004, and 21832001), and the Beijing National Laboratory for Molecular Sciences (Grant BNLMS-CXXM-201905).

Author affiliations: [a]Beijing National Laboratory for Molecular Sciences, College of Chemistry and Molecular Engineering, Peking University, Beijing 100871, China; and [b]State Key Laboratory for Physical Chemistry of Solid Surfaces, Collaborative Innovation Center of Chemistry for Energy Materials, National Engineering Laboratory for Green Chemical Productions of Alcohols-Ethers-Esters, College of Chemistry and Chemical Engineering, Xiamen University, Xiamen 361005, China

1. L. T. Mika, E. Cséfalvay, Á. Németh, Catalytic conversion of carbohydrates to initial platform chemicals: Chemistry and sustainability. *Chem. Rev.* **118**, 505–613 (2018).
2. Y. Liao *et al.*, A sustainable wood biorefinery for low-carbon footprint chemicals production. *Science* **367**, 1385–1390 (2020).
3. R. Gérardy, D. P. Debecker, J. Estager, P. Luis, J. M. Monbaliu, Continuous flow upgrading of selected C_2-C_6 platform chemicals derived from biomass. *Chem. Rev.* **120**, 7219–7347 (2020).
4. F. Subrizi, L. Benhamou, J. M. Ward, T. D. Sheppard, H. C. Hailes, Aminopolyols from carbohydrates: Amination of sugars and sugar-derived tetrahydrofurans with transaminases. *Angew. Chem. Int. Ed. Engl.* **58**, 3854–3858 (2019).
5. C. Xu, E. Paone, D. Rodríguez-Padrón, R. Luque, F. Mauriello, Recent catalytic routes for the preparation and the upgrading of biomass derived furfural and 5-hydroxymethylfurfural. *Chem. Soc. Rev.* **49**, 4273–4306 (2020).
6. J. Iglesias *et al.*, Advances in catalytic routes for the production of carboxylic acids from biomass: A step forward for sustainable polymers. *Chem. Soc. Rev.* **49**, 5704–5771 (2020).
7. R. L. Shahab *et al.*, A heterogeneous microbial consortium producing short-chain fatty acids from lignocellulose. *Science* **369**, eabb1214 (2020).
8. W. H. Faveere *et al.*, Toward replacing ethylene oxide in a sustainable world: Glycolaldehyde as a bio-based C_2 platform molecule. *Angew. Chem. Int. Ed. Engl.* **60**, 12204–12223 (2021).
9. A. V. Ellis, M. A. Wilson, Carbon exchange in hot alkaline degradation of glucose. *J. Org. Chem.* **67**, 8469–8474 (2002).
10. T. Deng, H. Liu, Promoting effect of SnO_x on selective conversion of cellulose to polyols over bimetallic Pt-SnO_x/Al_2O_3 catalysts. *Green Chem.* **15**, 116–124 (2013).
11. N. Ji *et al.*, Direct catalytic conversion of cellulose into ethylene glycol using nickel-promoted tungsten carbide catalysts. *Angew. Chem. Int. Ed. Engl.* **47**, 8510–8513 (2008).
12. Z. Tai, J. Zhang, A. Wang, M. Zheng, T. Zhang, Temperature-controlled phase-transfer catalysis for ethylene glycol production from cellulose. *Chem. Commun. (Camb.)* **48**, 7052–7054 (2012).
13. Y. Liu, C. Luo, H. Liu, Tungsten trioxide promoted selective conversion of cellulose into propylene glycol and ethylene glycol on a ruthenium catalyst. *Angew. Chem. Int. Ed. Engl.* **51**, 3249–3253 (2012).
14. M. Zheng, J. Pang, R. Sun, A. Wang, T. Zhang, Selectivity control for cellulose to diols: Dancing on eggs. *ACS Catal.* **7**, 1939–1954 (2017).
15. A. Wang, T. Zhang, One-pot conversion of cellulose to ethylene glycol with multifunctional tungsten-based catalysts. *Acc. Chem. Res.* **46**, 1377–1386 (2013).
16. N. Li *et al.*, Enhanced Ni/W/Ti catalyst stability from Ti–O–W linkage for effective conversion of cellulose into ethylene glycol. *ACS Sustain. Chem.& Eng.* **8**, 9650–9659 (2020).
17. N. Li, Y. Zheng, L. Wei, H. Teng, J. Zhou, Metal nanoparticles supported on WO_3 nanosheets for highly selective hydrogenolysis of cellulose to ethylene glycol. *Green Chem.* **19**, 682–691 (2017).
18. C. Li, G. Xu, X. Zhang, Y. Fu, Selectively chemocatalytic conversion of fructose to 1,2-propylene glycol over Ru-WO_x/hydroxyapatite catalyst. *Chin. J. Chem.* **38**, 453–457 (2020).
19. C. Liu *et al.*, Effect of WO_x on bifunctional Pd-WO_x/Al_2O_3 catalysts for the selective hydrogenolysis of glucose to 1,2-propanediol. *ACS Catal.* **5**, 4612–4623 (2015).
20. D. Chu *et al.*, One-pot hydrogenolysis of cellulose to bioethanol over Pd-Cu-WO_x/SiO_2 catalysts. *Fuel* **292**, 120311 (2021).
21. M. Yang *et al.*, One-pot production of cellulosic ethanol via tandem catalysis over a multifunctional Mo/Pt/WO_x catalyst. *Joule* **3**, 1937–1948 (2019).
22. H. Song *et al.*, Direct conversion of cellulose into ethanol catalysed by a combination of tungstic acid and zirconia-supported Pt nanoparticles. *Chem. Commun. (Camb.)* **55**, 4303–4306 (2019).
23. C. Li *et al.*, One-pot chemocatalytic transformation of cellulose to ethanol over Ru-WO_x/HZSM-5. *Green Chem.* **21**, 2234–2239 (2019).
24. N. Shi *et al.*, Production of lactic acid from cellulose catalyzed by easily prepared solid $Al_2(WO4)_3$. *Bioresour. Technol. Rep.* **5**, 66–73 (2019).
25. G. Zhao *et al.*, Ethylene glycol production from glucose over W-Ru catalysts: Maximizing yield by kinetic modeling and simulation. *AIChE J.* **63**, 2072–2080 (2017).
26. G. Zhao, M. Zheng, J. Zhang, A. Wang, T. Zhang, Catalytic conversion of concentrated glucose to ethylene glycol with semicontinuous reaction system. *Ind. Eng. Chem. Res.* **52**, 9566–9572 (2013).
27. Y. Liu, H. Liu, Kinetic insight into the effect of the catalytic functions on selective conversion of cellulose to polyols on carbon-supported WO_3 and Ru catalysts. *Catal. Today* **269**, 74–81 (2016).
28. J. Zhang *et al.*, Kinetic study of Retro-Aldol condensation of glucose to glycolaldehyde with ammonium metatungstate as the catalyst. *AIChE J.* **60**, 3804–3813 (2014).
29. N. Li *et al.*, Effect of the surface acid sites of tungsten trioxide for highly selective hydrogenation of cellulose to ethylene glycol. *Bioresour. Technol.* **264**, 58–65 (2018).
30. J. Chai *et al.*, Effect of tungsten surface density of WO_3-ZrO_2 on its catalytic performance in hydrogenolysis of cellulose to ethylene glycol. *RSC Advances* **7**, 8567–8574 (2017).
31. J. J. Wiesfeld, P. Peršolja, F. A. Rollier, A. M. Elemans-Mehring, E. J. M. Hensen, Cellulose conversion to ethylene glycol by tungsten oxide-based catalysts. *Mol. Catal.* **473**, 110400 (2019).
32. L. S. Ribeiro, J. Orfao, J. J. D. Orfao, M. F. R. Pereira, Hydrolytic hydrogenation of cellulose to ethylene glycol over carbon nanotubes supported Ru-W bimetallic catalysts. *Cellulose* **25**, 2259–2272 (2018).
33. S. Wang, J. Chen, L. Chen, Selective conversion of cellulose into ethylene glycol over metal-organic framework-derived multifunctional catalysts. *Catal. Lett.* **144**, 1728–1734 (2014).
34. Z. Tai *et al.*, Catalytic conversion of cellulose to ethylene glycol over a low-cost binary catalyst of Raney Ni and tungstic acid. *ChemSusChem* **6**, 652–658 (2013).
35. L. S. Ribeiro, J. J. M. Órfão, M. F. R. Pereira, Insights into the effect of the catalytic functions on selective production of ethylene glycol from lignocellulosic biomass over carbon supported ruthenium and tungsten catalysts. *Bioresour. Technol.* **263**, 402–409 (2018).
36. G. Pan *et al.*, Catalytic hydrogenation of corn stalk into polyol over Ni-W/MCM-41 catalyst. *Chem. Eng. J.* **299**, 386–392 (2016).
37. K. Fabicovicova, M. Lucas, P. Claus, From microcrystalline cellulose to hard- and softwood-based feedstocks: Their hydrogenolysis to polyols over a highly efficient ruthenium-tungsten catalyst. *Green Chem.* **17**, 3075–3083 (2015).
38. L. Zhou, A. Wang, C. Li, M. Zheng, T. Zhang, Selective production of 1,2-propylene glycol from Jerusalem artichoke tuber using Ni-$W_{(2)}$ C/AC catalysts. *ChemSusChem* **5**, 932–938 (2012).
39. Y. Liu, L. Chen, W. Zhang, H. Liu, Recyclable Cu salt-derived brønsted acids for hydrolytic hydrogenation of cellulose on Ru catalyst. *CCS Chem.*, 3419–3426 (2021).
40. A. Fukuoka, P. L. Dhepe, Catalytic conversion of cellulose into sugar alcohols. *Angew. Chem. Int. Ed. Engl.* **45**, 5161–5163 (2006).
41. A. Onda, T. Ochi, K. Yanagisawa, Selective hydrolysis of cellulose into glucose over solid acid catalysts. *Green Chem.* **10**, 1033 (2008).
42. S. Suganuma *et al.*, Hydrolysis of cellulose by amorphous carbon bearing SO_3H, COOH, and OH groups. *J. Am. Chem. Soc.* **130**, 12787–12793 (2008).
43. C. Luo, S. Wang, H. Liu, Cellulose conversion into polyols catalyzed by reversibly formed acids and supported ruthenium clusters in hot water. *Angew. Chem. Int. Ed. Engl.* **46**, 7636–7639 (2007).
44. J. Sun, H. Liu, Selective hydrogenolysis of biomass-derived xylitol to ethylene glycol and propylene glycol on supported Ru catalysts. *Green Chem.* **13**, 135–142 (2011).
45. M. Banu, S. Sivasanker, T. M. Sankaranarayanan, P. Venuvanalingam, Hydrogenolysis of sorbitol over Ni and Pt loaded on NaY. *Catal. Commun.* **12**, 673–677 (2011).
46. E. R. Cole, D. C. Craig, L. J. Fitzpatrick, D. B. Hibbert, J. D. Stevens, Structure and solution equilibria of D-glucose and D-mannose sulfite adducts. *Carbohydr. Res.* **335**, 1–10 (2001).
47. M. J. Kingmorris, A. S. Serianni, ^{13}C NMR studies of [1-^{13}C]Aldoses–empirical rules correlating pyranose ring configuration and conformation with ^{13}C chemical shifts and ^{13}C-^{13}C spin couplings. *J. Am. Chem. Soc.* **109**, 3501–3508 (1987).
48. T. Allscher, P. Klüfers, O. Labisch, On the basics of carbohydrate-metal chemistry: Complexes of palladium(II) with hydroxyaldehyde and -ketone hydrates. *Carbohydr. Res.* **342**, 1419–1426 (2007).
49. M. L. Hayes, N. J. Pennings, A. S. Serianni, R. Barker, Epimerization of aldoses by molybdate involving a novel rearrangement of the carbon skeleton. *J. Am. Chem. Soc.* **104**, 6764–6769 (1982).
50. J. P. Sauvage, J. F. Verchere, S. Chapelle, A multinuclear NMR spectroscopy study of the tungstate and molybdate complexes of D-fructose and L-sorbose. *Carbohydr. Res.* **286**, 67–76 (1996).
51. S. Chapelle, J. F. Verchere, ^{183}W NMR studies of tungstate complexes of carbohydrates. 1. Characterization of 2 structural types in the alditol series–evidence that the tungstate and molybdate threo complexes are not homologous. *Inorg. Chem.* **31**, 648–652 (1992).
52. S. Chapelle, J. P. Sauvage, J. F. Verchere, ^{183}W NMR studies of tungstate complexes of carbohydrates. 2. Competitive formation of erythro and threo complexes of alditols–characterization of a novel bis-dinuclear complex formed with perseitol. *Inorg. Chem.* **33**, 1966–1971 (1994).
53. M. Hlaibi, M. Hor, M. Riri, A. Benjjar, J. F. Verchere, Multinuclear ^{183}W and ^{13}C NMR and indirect photometry study for the identification and the characterization of new complexes of sugar acids. *J. Mol. Struct.* **920**, 310–322 (2009).
54. B. Ma *et al.*, Fabrication of $WO_{2.72}$/RGO nano-composites for enhanced photocatalysis. *RSC Advances* **7**, 2606–2614 (2017).
55 D. H. Murray, J. Prokop, Synthesis of deoxy sugars. I. New synthesis of 3-deoxy-D-glucose and 3-deoxy-D-mannose. *J. Pharm. Sci.* **54**, 1637 (1965).
56. J. R. Snyder, A. S. Serianni, Synthesis and n.m.r.-spectral analysis of unenriched and [1-^{13}C]-enriched 5-deoxypentoses and 5-O-methylpentoses. *Carbohydr. Res.* **163**, 169–188 (1987).
57. G. Kresse, J. Furthmüller, Efficiency of ab-initio total energy calculations for metals and semiconductors using a plane-wave basis set. *Comput. Mater. Sci.* **6**, 15–50 (1996).
58. G. Kresse, J. Furthmüller, Efficient iterative schemes for ab initio total-energy calculations using a plane-wave basis set. *Phys. Rev. B Condens. Matter* **54**, 11169–11186 (1996).
59. G. Kresse, J. Hafner, Ab initio molecular dynamics for open-shell transition metals. *Phys. Rev. B Condens. Matter* **48**, 13115–13118 (1993).
60. G. Kresse, J. Hafner, Ab initio molecular-dynamics simulation of the liquid-metal-amorphous-semiconductor transition in germanium. *Phys. Rev. B Condens. Matter* **49**, 14251–14269 (1994).
61. G. Kresse, D. Joubert, From ultrasoft pseudopotentials to the projector augmented-wave method. *Phys. Rev. B Condens. Matter Mater. Phys.* **59**, 1758 (1999).
62. J. P. Perdew, K. Burke, M. Ernzerhof, Generalized gradient approximation made simple. *Phys. Rev. Lett.* **77**, 3865–3868 (1996).
63. S. Grimme, S. Ehrlich, L. Goerigk, Effect of the damping function in dispersion corrected density functional theory. *J. Comput. Chem.* **32**, 1456–1465 (2011).
64. P. M. Oliver, S. C. Parker, R. G. Egdell, F. H. Jones, Computer simulation of the surface structures of WO_3. *J. Chem. Soc., Faraday Trans.* **92**, 2049–2056 (1996).
65. Y. Xi, Q. Zhang, H. Cheng, Mechanism of hydrogen spillover on WO_3 (001) and formation of H_xWO_3 (x= 0.125, 0.25, 0.375, and 0.5). *J. Phys. Chem. C* **118**, 494–501 (2014).
66. G. Henkelman, H. Jónsson, Improved tangent estimate in the nudged elastic band method for finding minimum energy paths and saddle points. *J. Chem. Phys.* **113**, 9978–9985 (2000).
67. G. Henkelman, H. Jónsson, A dimer method for finding saddle points on high dimensional potential surfaces using only first derivatives. *J. Chem. Phys.* **111**, 7010–7022 (1999).